Supplementary material

Prediction of Secondary Organic Aerosol from the Multiphase Reaction of Gasoline Vapor by Using Volatility-Reactivity Base Lumping

Sanghee Han and Myoseon Jang*
Department of Environmental Engineering Science, University of Florida, Gainesville, Florida, USA

Correspondence to: Myoseon Jang (mjang@ufl.edu)

This file includes:
5 Sections
2 Tables
7 Figures
References

Section S1. Gasoline fuel composition and its application to Carbon Bond 6

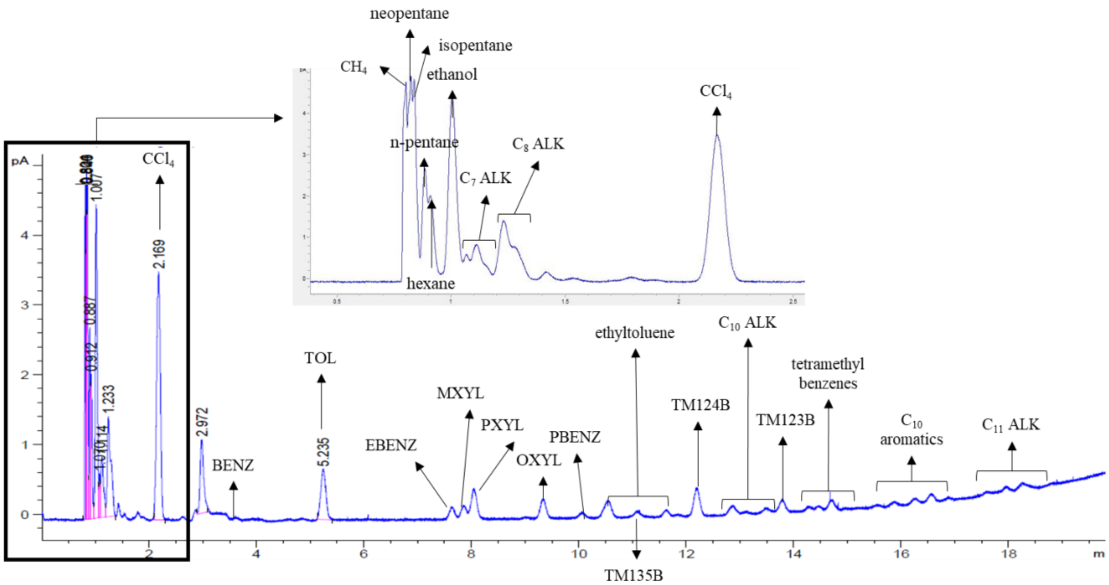

Figure S1. The GC-FID chromatogram of gasoline fuel.

Figure S1 illustrates the GC-FID chromatogram of gasoline vapor. To separate GC peaks, the oven temperature was held at 35℃ for 3 minutes and increased to 120℃ at 5℃ min^{-1}. The aromatic HC fraction to total hydrocarbons was about 30%. The reaction rate constants and gas mechanisms used in CB6r3 are as follows.

Table S1. Reactions of aromatic HCs of this study with an OH radical and their rate constants

Aromatic HC	Reaction mechanisms	Rate constants	References[a)]
benzene	BENZENE + OH → 0.530*CRES + 0.352*BZO2 + 0.352*RO2 + 0.118*OPEN + 0.118*OH + 0.530*HO2 + BENZRO2	$2.30\times10^{-12}e^{-190.00/T}$	CB6r3[1]
toluene	TOL + OH → 0.180*CRES + 0.650*TO2 + 0.720*RO2 + 0.100*OPEN + 0.100*OH + 0.070*XO2H + 0.180*HO2 + TOLRO2	$1.80\times10^{-12}e^{340.00/T}$	CB6r3[1]
ethylbenzene	EBENZ + OH → 0.180*CRES + 0.650*TO2 + 0.720*RO2 + 0.100*OPEN + 0.100*OH + 0.070*XO2H + 0.180*HO2 + TOLRO2 PAR + OH → XPAR	7.00×10^{-12} 8.1×10^{-13}	MCM v3.3.1[2] CB6r3[1]
propylbenzene	PBENZ + OH → 0.180*CRES + 0.650*TO2 + 0.720*RO2 + 0.100*OPEN + 0.100*OH + 0.070*XO2H + 0.180*HO2 + TOLRO2 2PAR + 2OH → 2XPAR	5.8×10^{-12} 8.1×10^{-13}	MCM v3.3.1[2] CB6r3[1]
o-xylene	OXYL + OH → 0.155*CRES + 0.544*XLO2 + 0.602*RO2 + 0.244*XOPN + 0.244*OH + 0.058*XO2H + 0.155*HO2 + XYLRO2	1.36×10^{-11}	MCM v3.3.1[2]
m-xylene	MXYL + OH → 0.155*CRES + 0.544*XLO2 + 0.602*RO2 + 0.244*XOPN + 0.244*OH + 0.058*XO2H + 0.155*HO2 + XYLRO2	2.31×10^{-11}	MCM v3.3.1[2]
p-xylene	PXYL + OH → 0.155*CRES + 0.544*XLO2 + 0.602*RO2 + 0.244*XOPN + 0.244*OH + 0.058*XO2H + 0.155*HO2 + XYLRO2	1.43×10^{-11}	MCM v3.3.1[2]
TM123B	TM123B + OH → 0.155*CRES + 0.544*XLO2 + 0.602*RO2 + 0.244*XOPN + 0.244*OH + 0.058*XO2H + 0.155*HO2 + XYLRO2 PAR + OH → XPAR	3.27×10^{-11} 8.1×10^{-13}	MCM v3.3.1[2] CB6r3
TM124B	TM124B + OH → 0.155*CRES + 0.544*XLO2 + 0.602*RO2 + 0.244*XOPN + 0.244*OH + 0.058*XO2H + 0.155*HO2 + XYLRO2 PAR + OH → XPAR	3.25×10^{-11} 8.1×10^{-13}	MCM v3.3.1[2] CB6r3[1]
TM135B	TM125B + OH → 0.155*CRES + 0.544*XLO2 + 0.602*RO2 + 0.244*XOPN + 0.244*OH + 0.058*XO2H + 0.155*HO2 + XYLRO2 PAR + OH → XPAR	5.67×10^{-11} 8.1×10^{-13}	MCM v3.3.1[2] CB6r3[1]
ethyltoluenes	Treated as a OXYL + PAR		
tetramethylbenzenes	Treated as a TM123B + PAR		

[a)] 1: (Yarwood et al., 2010), 2: (Jenkin et al., 2012)

Section S2. Model parameters in the absence of gas-wall partitioning.

S2.1. near explicit UNIPAR-GWP

The UNIPAR model was coupled with the Master Chemical Mechanism (MCM v3.3.1) to explicitly treat SOA formation by using individual chemical properties (i.e., molecular weight, O:C ratio, hydrogen bonding) of oxygenated products. The UNIPAR simulation was performed in the box model platform by using the Dynamically Simple Model of Atmospheric Chemical Complexity (DSMACC)(Emmerson and Evans, 2009) platform integrated with the Kinetic PreProcessor (KPP)(Damian et al., 2002). The oxidation products from the MCM mechanisms were explicitly integrated with the UNIPAR model.

To assess the impact if gas-wall partitioning (GWP) on SOA formation, UNIPAR model was coupled with GWP model (UNIPAR-GWP). In UNIPAR-GWP, both gas-particle partitioning and GWP were kinetically treated by using the absorption rate constants (kon) and desorption rate constants ($koff$) of organic species *i*, in the *or*, *in*, and *w* phases. The SOA growth via in-particle chemistry was also kinetically treated as the second-order dimerization reaction of condensed organics with aerosol phase reaction rate constants ($k_{o,i}$ for organic phase and $k_{AC,i}$ for the inorganic phase).(Odian, 2004) The kinetic mechanisms associate with the oxidation product *i* were listed as:

1) Gas phase oxidation (MCM v3.3.1)

   $I_g + \mathrm{OH} \xrightarrow{k_{OH,i}} I'_g$

2) Gas-particle partitioning (into the organic phase)

   $I_g \xrightarrow{kon_{or,i}} I_{or}$

   $I_{or} \xrightarrow{koff_{or,i}} I_g$

3) Gas-particle partitioning (into the inorganic phase)

   $I_g \xrightarrow{kon_{in,i}} I_{in}$

   $I_{in} \xrightarrow{koff_{in,i}} I_g$

4) Gas-wall partitioning (GWP)

   $I_g \xrightarrow{kon_{w,i}} I_w$

   $I_w \xrightarrow{koff_{w,i}} I_g$

5) In-particle chemistry (organic phase)

   2nd order reaction

6) In-particle chemistry (inorganic phase)

   2nd order reaction

In this study, reversibility of oligomerization was not considered. Figure S2 illustrates the simple structure of UNIPAR-GWP.

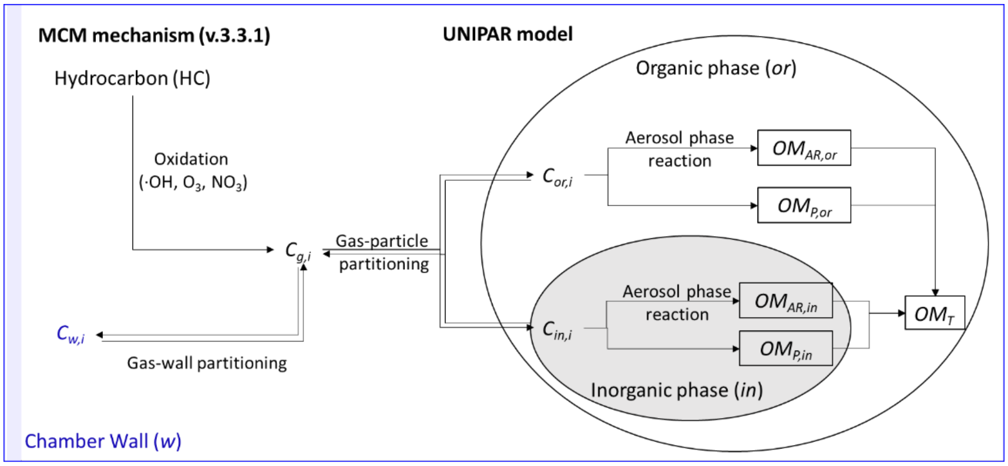

Figure S2. The structure of the UNIPAR-GWP model, simulated to predict the impact of GWP on aromatic SOA formation. *C* denotes the concentration of the organic compound (*i*) in gas phase (g), organic phase (or), inorganic phase (in), and chamber wall phase (w). $C_{g,i}$ is simulated using the gas kinetic mechanisms (MCM v3.3.1). The gas-phase reactions, multiphase partitioning processes, and aerosol-phase reactions to form the SOA mass are integrated into a chemical solver under the Dynamically Simple Model of the Atmospheric Chemical Complexity (DSMACC) platform.

The chemical properties were explicitly treated for partitioning processes. The physicochemical parameters of oxygenated products resulting from the MCM mechanism were obtained from individual species. For GWP, the physicochemical parameters (hydrogen bond donor ($H_{d,i}$), hydrogen bond acceptor ($H_{a,i}$), dipolarity/polarizability (S_i), and polarizability (P_i)) of *i* were obtained from PaDEL-descriptor (Yap, 2011) and applied to calculate the GWP parameter (Han and Jang, 2020). The gas-wall partitioning coefficient (K_w) and absorption rate constant ($kon_{w,i}$) are two important GWP parameters which can determine the deposition of organic vapor to the chamber wall. K_w is a unitless partitioning coefficient derived from the traditional partitioning coefficient by multiplying organic matter absorbed on the chamber wall (OM_{wall}) (Han and Jang, 2020;Krechmer et al., 2016):

$$K_{w,i} = \frac{7.501RTOM_{wall}}{10^9 MW_{OM}\gamma_{w,i}p^{\circ}_{L,i}} \tag{S1}$$

where MW_{OM} is the molecular weight of OM_{wall} and $\gamma_{w,i}$ is the activity coefficient of *i* in the wall phase. R (8.314 J mol^{-1} K^{-1}) is the ideal gas constant, and T (K) is the temperature. $p^{\circ}_{L,i}$ denotes the vapor pressure of *i*. The absorption rate constant ($kon_{w,i}$) of *i* to the wall is expressed as a fractional loss rate with the accommodation coefficient ($\alpha_{wall,i}$)(McMurry and Grosjean, 1985) of *i* to the organic matter on the chamber wall:

$$kon_{w,i} = \left(\frac{A}{V}\right)\frac{\alpha_{wall,i}\bar{v}_i/4}{1+\frac{\pi\alpha_{wall,i}\bar{v}_i}{8\sqrt{K_e D}}} \tag{S2}$$

where *D* (1.0×10^{-6} m^2 s^{-1}) and K_e (0.12 s^{-1}) are the diffusion coefficient and the coefficient of eddy diffusion, respectively. $\bar{v}_i$ is the gas molecules' mean thermal speed of *i*. A is the surface area and V is the volume of the chamber. The important parameters, activity coefficient of *i* to the wall ($\gamma_{w,i}$) to calculate K_w and accommodation coefficient ($\alpha_{wall,i}$) to calculate k_{on}, were estimated by applying a quantitative structure activity relationship (QSAR) employing organic vapors' physicochemical properties. QSAR models are semiempirically determined by using the experimental data that measured time series gas-phase concentrations of SVOCs in the UF-APHOR chamber to predict $\gamma_{w,i}$ and $\alpha_{wall,i}$:

$$\ln(\gamma_{w,i}) = 2.25e^{0.0007RH}H_{d,i} + 0.79e^{0.022RH}H_{a,i} + 0.13e^{0.0025RH}P_i - 6.54e^{0.0047RH} \tag{S3}$$

$$\ln(\alpha_{wall,i}) = -0.33H_{d,i} - 3.00H_{a,i} - 0.05P_i - 0.61S_i - 9.69 \tag{S4}$$

where $H_{d,i}$, $H_{a,i}$, S_i, and P_i indicate the hydrogen bond donor, hydrogen bond acceptor, dipolarity/polarizability, and polarizability, respectively (Abraham and McGowan, 1987;Abraham et al., 1991;Platts et al., 1999).

The UNIPAR-GWP model was limited to simulate individual compounds of data due to the complexity of mechanism, and thus it was applied to correct the SOA parameters for GWP bias. To improve the SOA parameters, aerosol phase reaction rate constant ($k_{o,i}$) was semiempirically determined by including the GWP mechanism to predict the SOA data generated from the UF-APHOR chamber.

S2.2. Simulation of aromatic SOA using UNIPAR-CB6r3

The chamber experiments were conducted under various seed conditions, such as NS (non-seed), SA (sulfuric acid seeded), wAS (wet ammonium sulfate seeded), and SO_2, to test SOA parameters and evaluate the feasibility of the UNIPAR-CB6r3 model. Experimental conditions for each chamber experiment are summarized in the Table S2.

Table S2. Experimental conditions of the chamber studies.

Precursor	Date[a]	Initial condition					Y_{SOA}[e] (%)	RH[f] (%)	Temp. (K)	Figure
		HC (ppb)	NO_x (HONO) (ppb)	Seeded aerosol[c] (ppb or μg m^{-3})	HC/NO_x (ppbC/ppb)	OM_0[d] (μg m^{-3})				
Benzene	05/31/20 W	515	680 (125)	-	4.2	5	3.8	37-99	295-321	2, S4(c)
	06/17/20 E	496	648 (134)	SA (50)	4.6	5	9.0	22-91	291-320	2
toluene	06/25/20 E	198	350(160)	-	5.0	2	2.6	21-70	296-321	2, S3(a), S4(a)
	02/23/2019 E	104	76 (76)	wAHS (250)	9.6	2	20.2	27-79	293-318	2, S4(b)
	02/23/2019 W	120	65(65)	wAS (350)	12.9	2	19.2	34-86	294-315	2, S4(b)
ethylbenzene	12/10/17 E[b]	131	363 (13)	SO_2 (39)	2.7	3	10.1	20-83	271-298	2
	12/10/17 W[b]	128	363 (15)	-	2.8	3	4.1	33-86	272-295	2
propylbenzene	03/28/18 E[b]	87	264 (36)	SO_2 (54)	3.0	3	7.1	11-43	285-312	2, S4(f)
	03/28/18 W[b]	88	248 (33)	-	3.2	3	4.6	16-51	285-312	2, S4(f)
m-xylene	11/27/2018 E	114	272	SA (80)	3.4	2	6.0	31-90	277-297	2, S3(d), S4(e)
	11/27/2018 W	117	274	-	3.4	2	2.0	51-93	277-295	2, S4(e)
o-xylene	10/28/2018 E	131	289	SA (70)	3.6	2	6.6	14-66	281-310	2, S3(b), S4(d)
	10/28/2018 W	128	294	wAS (80)	3.5	2	4.0	36-93	282-310	2, S4(d)
p-xylene	01/21/2019 E	121	86	SA (70)	11.3	2	11.6	15-70	271-299	2
	01/21/2019 W	119	79	-	12.1	2	3.1	26-74	272-299	2
1,2,3TMB	9/25/2018 E	148	353	SA (50)	3.8	2	5.4	12-39	296-322	2
	9/25/2018 W	141	335	-	3.8	2	1.0	16-41	296-321	2
1,2,4TMB	9/8/2018 E	115	275	SA (70)	3.8	2	1.9	13-44	294-321	2, S3(e), S4(h)
	9/8/2018 W	115	269	-	3.8	2	0.9	19-50	295-319	2, S4(h)
1.3.5TMB	9/10/2019 E	210	600	-	3.2	5	1.1	13-40	296-322	2, S4(g)
	9/10/2019 W	211	617	SA (50)	3.1	5	3.4	23-50	297-319	2, S4(g)

a. "E" or "W" that follows the experiment date represents the east or west chamber for the UF APHOR, respectively.
b. The SOA data obtained from (Zhou et al., 2019).
c. "SA", "wAS", or "wAHS" denotes that the experiment with sulfuric-acid aerosol, wet ammonium-sulfate aerosol, or wet ammonium-hydrogen sulfate aerosol is directly injected to the chamber, respectively. SO_2 (in the unit of ppb) was injected into the chamber to generate sulfuric acidic seeds under the sun light.
d. The pre-existing organic matter (OM_0) is determined based on the measured organic matter in the chamber before experiment and applied to the simulation for the initial condition.
e. SOA yield is estimated using $Y_{SOA} = \Delta OM_T/\Delta HC$. Yield in the table was estimated when SOA mass reached to the maximum over the course of the experiments.
f. The accuracy of relative humidity (RH) is 5 %. The accuracy of temperature is 0.5 K.

The time profiles of the simulated concentration of NO, NO_2, O_3, and aromatic HC with CB6r3 mechanism under the experimental conditions (Table S2) are illustrated in Fig. S3. The simulated aromatic SOA mass with UNIPAR-CB6r3 model under the experimental conditions (Table S2) is shown in Fig. S4.

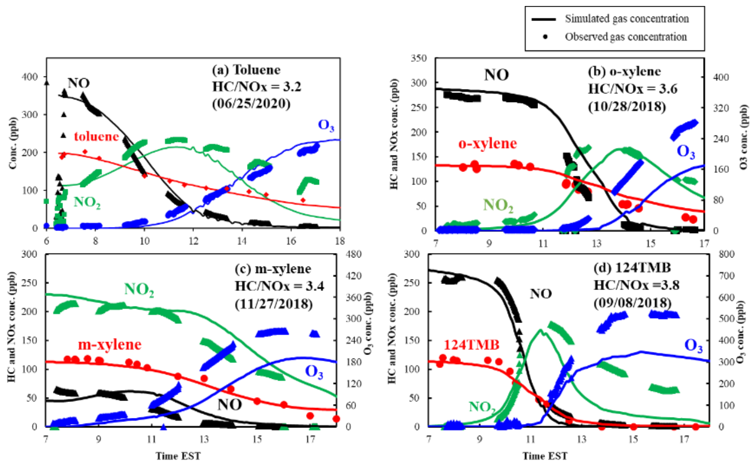

Figure S3. Observed (symbol) and simulated (line) concentration of NO, NO_2, O_3, and HC for the photooxidation of individual aromatic HCs. The environmental conditions of the chamber experiment are described in Table S2.

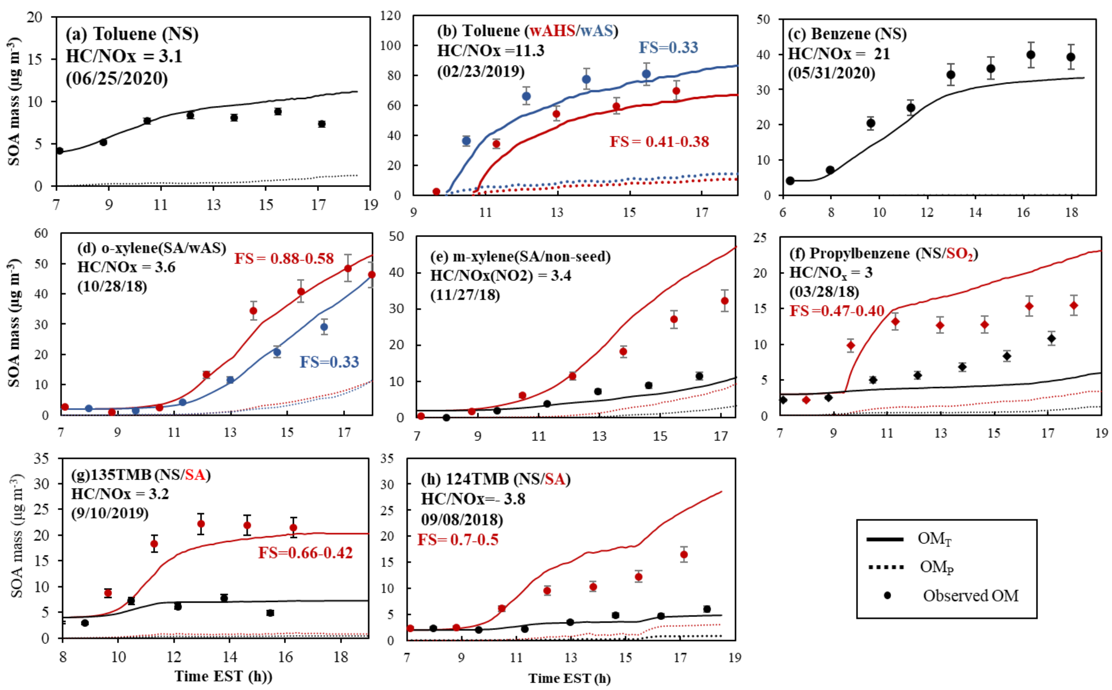

Figure S4. Observed (plot) and simulated (line) SOA mass in the chamber studies of aromatic HCs. The simulated OM_T (solid line) and OM_P (dotted line) are illustrated. Particle loss of experimental data onto the chamber wall was corrected. The ranges of FS are presented for experiment under the acidic condition to indicate aerosol acidity over the course of the experiment. The error (9%) associated with SOA mass was estimated with the instrumental error originating from the OC/EC analyzer.

Overall, the simulated concentrations of aromatic SOA, NO, NO_2, O_3, and HC with UNIPAR-CB6r3 agrees with the observed values in the chamber studies.

Section S3. Impact of GWP on aromatic SOA formation

Figure S5 illustrates the SOA mass (C_{SOA}, μg m^{-3}) in the absence of GWP bias and the SOA mass ($C_{SOA,wall}$, μg m^{-3}) predicted in the presence of GWP for 10 different aromatic HCs under various seed conditions (no-seed, NS; wet ammonium sulfate, wAS; wet ammonium hydrogen sulfate, wAHS) at a given temperature (298K) and RH (60%) under the specific sunlight intensity (Fig. S6) measured from the UF-APHOR chamber on 06/19/2015. The pre-existing organic matter was set as 3 μg m^{-3}, and the NO_x concentration was controlled as (a) high NO_x level (HC/NO_x = 3 ppbC/ppb) and (b) low NO_x level (HC/NO_x = 10 ppbC/ppb). To evaluate the potential SOA formation, C_{SOA} and $C_{SOA,wall}$ were obtained at 5PM with same consumption of HC (100 μg m^{-3}), and the initial concentrations of HCs set differently.

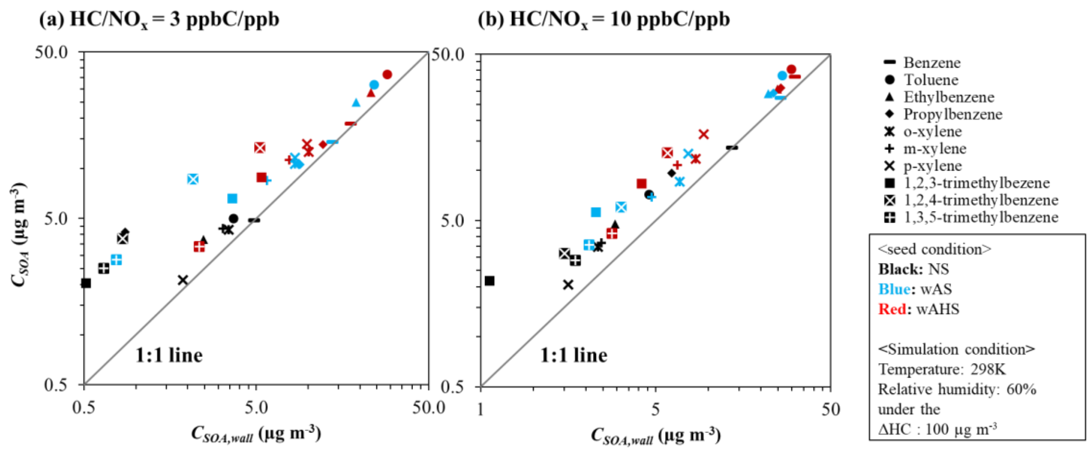

Figure S5. The simulated C_{SOA} and $C_{SOA,wall}$ for 10 different aromatic HCs at the given reference conditions. The SOA formation is simulated at the 298K and 60% at a given sunlight intensity (Fig. S6). The concentration of initial HC is determined to consume 100 μg m^{-3} of HC at 5PM. The initial HC ppbC/NO_x ppb sets to 3 and 10 for high NO_x level and low NO_x level, respectively. SOA masses are also obtained at 5PM. The color of the symbol indicates the seed conditions: black, blue, and red for non-seeded (NS), wet ammonium sulfate (wAS), and wet ammonium hydrogen sulfate (wAHS), respectively.

As seen in Fig. S5, the SOA mass in the absence of GWP is plotted to the SOA mass in the presence of GWP from photooxidation of 10 different aromatic HCs. The more deviated plot from the 1:1 line indicates the larger impact of GWP on SOA formation. The GWP bias was the least for benzene SOA formation. In the presence of wet inorganic seed, the impact of GWP on SOA mass was insignificant. These small impacts of GWP on SOA formation in the presence of wet inorganic seed indicate that the enhancement of aerosol growth via aerosol phase reaction can cause the less GWP effect on SOA formation. This tendency agreed to the previously reported results (Krechmer et al., 2020;Zhang et al., 2014). For example, Krechmer et al. (2020) suggested the possibility that the higher amounts of seed can help partially overcome losses to the walls. Zhang et al. (2014) reported that the larger seed particle surface area can reduce the significance of GWP on SOA yield.

Section S4. Reference sunlight intensity

The sunlight intensity illustrated in Fig. S6 was measured on 06/19/2015 in the UF-APHOR and applied as a reference sunlight intensity for the simulation.

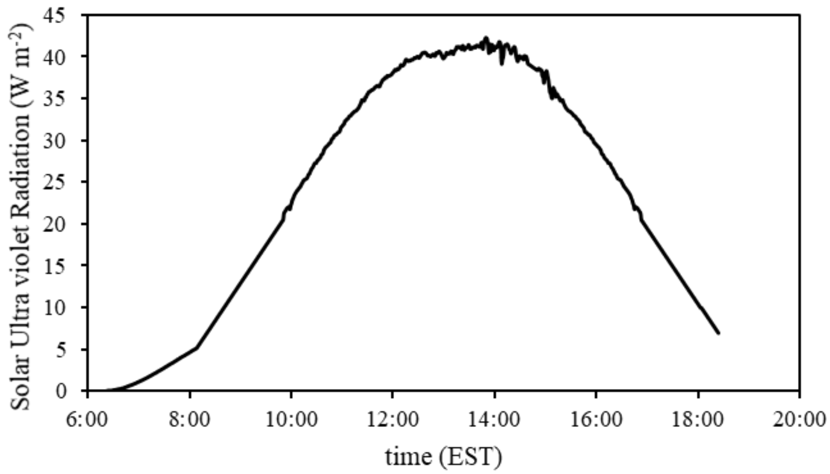

Figure S6. Time profile of sunlight total ultra-violet radiation (TUVR) measured in the UF-APHOR on 06/19/2015.

Section S5. SOA simulation using CMAQ-AE7 aerosol module

To compare the SOA simulation results between UNIPAR-CB6r3 and CMAQ-AE7, 2 gasoline SOA data generated in UF-APHOR in the absence of wet inorganic seed were simulated with both models. In CMAQ-AE7, the first order oligomerization reaction of organic species is included in gas mechanisms with the rate constant as 9.5×10^{-6} molecules s^{-1} cm^{-3}, while UNIPAR-CB6r3 treats the oligomerization as the second order self-dimerization reaction. In Fig. S7, the SOA simulation with CMAQ-AE7 is compared to the SOA data generated from the photooxidation of gasoline vapor. The simulated gasoline SOA using UNIPAR-CB6r3 is shown in Fig. 3 in the manuscript.

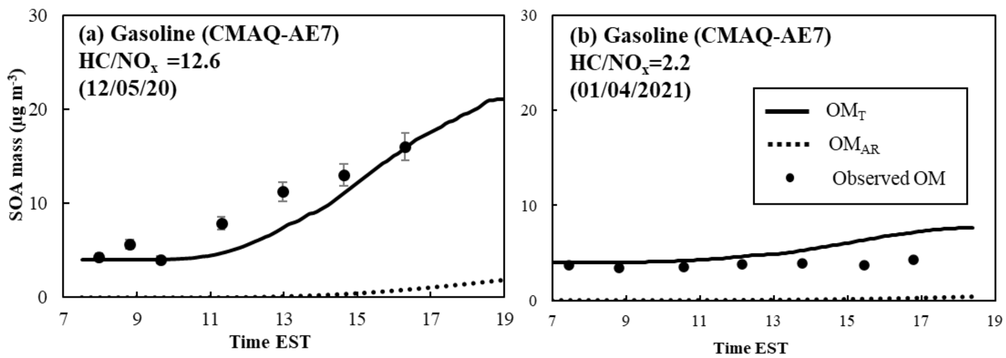

Figure S7. Simulation of gasoline SOA mass by using the CMAQ-AE7 module against SOA data generated without inorganic seed in the UF-APHOR chamber (Table 1).

References

Abraham, M., and McGowan, J.: The use of characteristic volumes to measure cavity terms in reversed phase liquid-chromatography, Chromatographia, 23, 243-246, 10.1007/BF02311772, 1987.

Abraham, M., Whiting, G., Doherty, R., and Shuely, W.: Hydrogen-bonding. 16. A new solute solvation parameter, Pi-2(H), from Gas-Chromatographic data, Journal of Chromatography, 587, 213-228, 10.1016/0021-9673(91)85158-C, 1991.

Damian, V., Sandu, A., Damian, M., Potra, F., and Carmichael, G. R.: The kinetic preprocessor KPP-a software environment for solving chemical kinetics, Computers & Chemical Engineering, 26, 1567-1579, 2002.

Emmerson, K., and Evans, M.: Comparison of tropospheric gas-phase chemistry schemes for use within global models, Atmospheric Chemistry and Physics, 9, 2009.

Han, S., and Jang, M.: Simulating the impact of gas-wall partitioning on SOA formation using the explicit gas mechanism integrated with aqueous reactions containing electrolytes, Science of The Total Environment, 748, 141360, 2020.

Jenkin, M., Wyche, K., Evans, C., Carr, T., Monks, P., Alfarra, M., Barley, M., McFiggans, G., Young, J., and Rickard, A.: Development and chamber evaluation of the MCM v3.2 degradation scheme for beta-caryophyllene, Atmospheric Chemistry and Physics, 12, 5275-5308, 10.5194/acp-12-5275-2012, 2012.

Krechmer, J., Pagonis, D., Ziemann, P., and Jimenez, J.: Quantification of Gas-Wall Partitioning in Teflon Environmental Chambers Using Rapid Bursts of Low-Volatility Oxidized Species Generated in Situ, Environmental Science & Technology, 50, 5757-5765, 10.1021/acs.est.6b00606, 2016.

Krechmer, J. E., Day, D. A., and Jimenez, J. L.: Always Lost but Never Forgotten: Gas-Phase Wall Losses Are Important in All Teflon Environmental Chambers, Environmental Science & Technology, 54, 12890-12897, 2020.

McMurry, P., and Grosjean, D.: Gas and aerosol wall losses in Teflon film smog chambers, Environmental Science & Technology, 19, 1176-1182, 10.1021/es00142a006, 1985.

Odian, G.: Principles of Polymerization, 4th ed., A JOHN WILEY & SONS, INC., New York, 2004.

Platts, J., Butina, D., Abraham, M., and Hersey, A.: Estimation of molecular linear free energy relation descriptors using a group contribution approach, Journal of Chemical Information and Computer Sciences, 39, 835-845, 10.1021/ci980339t, 1999.

Yap, C.: PaDEL-Descriptor: An Open Source Software to Calculate Molecular Descriptors and Fingerprints, Journal of Computational Chemistry, 32, 1466-1474, 10.1002/jcc.21707, 2011.

Yarwood, G., Jung, J., Whitten, G. Z., Heo, G., Mellberg, J., and Estes, M.: Updates to the Carbon Bond mechanism for version 6 (CB6), 9th Annual CMAS Conference, Chapel Hill, NC, 2010, 11-13,

Zhang, X., Cappa, C., Jathar, S., Mcvay, R., Ensberg, J., Kleeman, M., and Seinfeld, J.: Influence of vapor wall loss in laboratory chambers on yields of secondary organic aerosol, Proceedings of the National Academy of Sciences of the United States of America, 111, 5802-5807, 10.1073/pnas.1404727111, 2014.

Zhou, C., Jang, M., and Yu, Z.: Simulation of SOA formation from the photooxidation of monoalkylbenzenes in the presence of aqueous aerosols containing electrolytes under various NOx levels, Atmospheric Chemistry and Physics, 19, 5719-5735, 2019.